Compressive damage modeling of fiber-reinforced composite laminates using 2D higher-order layer-wise models

# Compressive damage modeling of fiber-reinforced composite laminates using 2D higher-order layer-wise models

M.H. Nagaraj[1], J. Reiner[2], R. Vaziri[3], E. Carrera[1], and M. Petrolo*[1]

[1]MUL[2] Group, Department of Mechanical and Aerospace Engineering, Politecnico di Torino, Corso Duca degli Abruzzi 24, 10129 Torino, Italy
[2]School of Engineering, Deakin University, Geelong, Australia
[3]Composites Research Network, The University of British Columbia, Vancouver, Canada

Submitted to

Composites Part B: Engineering

*Author for correspondence:*
M. Petrolo, Associate Professor
MUL[2] Group, Department of Mechanical and Aerospace Engineering,
Politecnico di Torino,
Corso Duca degli Abruzzi 24,
10129 Torino, Italy,
tel: +39 011 090 6845,
fax: +39 011 090 6899,
e-mail: marco.petrolo@polito.it

## *Abstract*

*A refined progressive damage analysis of fiber-reinforced laminated composites subjected to compressive loads is presented here. The numerical analysis exploits higher-order theories developed using the Carrera Unified Formulation, specifically 2D plate theories with Lagrange polynomials to enhance the kinematic approximation through each ply's thickness resulting in a layer-wise structural model. The CODAM2 material model, based on continuum damage mechanics, governs the intralaminar composite damage. The Hashin criteria and the crack-band approach provides failure initiation and propagation, respectively. Fiber micro-buckling and kinking is taken into account via the use of nonlinear post-peak softening models. It is shown that linear-brittle stress-strain softening is effective for accurate compressive strength predictions. A series of numerical assessments on coupon-level composite laminates is carried out to verify the proposed numerical framework while its validation is demonstrated by successfully applying the numerical tool to test cases for which experimental data is available from the literature. Various through-the-thickness structural models are evaluated to provide insights for proper modeling.*



**Keywords**: CODAM2, CUF, explicit nonlinear analysis, layer-wise elements, continuum damage analysis

# 1 Introduction

Fiber-reinforced laminated structures have been successfully deployed in the aerospace, automotive, and maritime sectors due to their high specific strength and stiffness. The low compressive strength of composites is a limiting factor in fully harnessing such material systems' capabilities. It may be critical in various scenarios, such as in crush or impact analyses, or the determination of the bearing strength of pin-bolted joints. Therefore, the detailed study of the compressive behavior of laminated composites is a crucial step towards the safe and reliable design of composite structures. Composite structures' behavior under compressive loading is significantly different - and more complex - than under tensile loading.

A crucial factor in determining composites' response under compression is the presence of manufacturing imperfections, such as fiber misalignment and microstructural voids [1]. For instance, Wisnom reported a significant reduction of the compressive strength even for small misalignments of the fibers [2]. Such manufacturing imperfections lead to various damage mechanisms in composites under compression. The most common failure modes include fiber buckling and kinking, and longitudinal splitting due to debonding of the fiber/matrix interface [3–5]. Failure mechanisms often interact with each other, leading to complex pathways for progressive damage and eventual failure. A detailed overview of the failure of composites subjected to compression is available in [6, 7].

Virtual testing approaches, in which numerical simulations predict composite laminates' response under compression, are emerging to support and reduce experimental testing. Failure initiation and propagation require damage models. Such models are generally of two types: discrete damage models (DDM) and continuum damage models (CDM). DDM explicitly accounts for the formation of intralaminar cracks within the ply, using techniques such as cohesive interface elements or the eXtended finite element method ($x$-FEM), to handle discontinuities within the finite element (FE) mesh. Such techniques lead to models that can accurately predict the crack propagation and with high fidelity, but at the cost of significant computational effort. Some examples of the application of DDM to compressive damage modeling include the analysis of static bearing failure in laminated composites [8], and the compression-after-impact (CAI) tests of carbon-fiber-reinforced polymers (CFRP) [9]. CDM techniques remain a prevalent approach due to their ease of implementation and reduced computational overheads compared to DDM. In CDM approaches, intralaminar cracks are smeared out within the FE domain, and their effects are accounted for via damage parameters quantifying the reduction of the material stiffness. Such models lead to a good compromise between computational cost and solution accuracy, and are thus used in most of the works dealing with composite damage modeling. Most material models available in the literature generally focus on progressive damage analysis under tensile loads, and the application of these models for the simulation of compressive tests is relatively scarce. Some examples of the use of CDM techniques for the compressive damage modeling of composites include [10–12].

The computational costs associated with progressive damage analysis of composite structures can be prohibitive, even considering the relative efficiency of CDM models, especially for larger structures. This is usually due to

the requirement of refined, often 3D, meshes, to obtain an accurate stress field, which are important inputs to the nonlinear material model. Various techniques have been proposed in the literature, to improve the computational efficiency of such analyses. A popular approach is solid/shell coupling, where the global structure consists of shell elements, and solid elements are present only in the region where damage may occur [13]. Similarly, global/local techniques are useful to study progressive damage and failure in composites [14, 15]. In recent years, continuum shell models have emerged as an alternative to 3D elements for these problems [16–18]. The current work addresses computational costs and accuracy by using higher-order structural models developed using the Carrera Unified Formulation (CUF) [19]. Such an approach can accurately evaluate 3D stress fields in a computationally efficient manner [20]. CUF has been used in recent years for the development of a numerical platform for the nonlinear analysis of beams [21], contact analysis of laminated and thin-walled structures [22, 23], progressive tensile damage analysis of composites [24], and, more recently, low-velocity impact analysis [25]. The present paper extends the findings in progressive damage modeling under tension [24], to composites loaded in compression. The nonlinear material behavior is described via the COmposite DAMage model (CODAM), an intralaminar damage model based on continuum damage mechanics, which was originally developed for the macroscopic sub-laminate level modeling of composites [26]. The CODAM material model was successfully applied to the compressive damage analysis of composites [27], and the axial crush simulation of braided composite tubes [28]. The second generation of the model, termed CODAM2, devolves the sub-laminate strain-softening response into equivalent stress-strain responses in the principal ply directions [29, 30], and has been implemented in the commercial FE solver LS-DYNA as MAT-219 [18, 31, 32]. The current work aims to combine CUF-based structural models with the CODAM2 material model to develop a numerical framework for the efficient and accurate mesoscopic progressive damage analysis of composite structures in compression. The focus is on evaluating the effect of higher-order terms in 2D theories and providing insights for a proper modeling strategy. 2D models can lead to significant reductions in the computational overheads compared to 3D, but refinements are necessary to retain the same accuracy [24, 25]. The refinement process must tackle several characteristics of composites that are particularly relevant for evaluating stress fields and damage initiation and progression, such as anisotropy, shear deformability, and continuity of transverse stress fields [33].

This article is organized as follows - Section 2 provides a brief overview of the FE formulation of higher-order structural theories based on CUF while the CODAM2 material model for compressive damage modeling is described in Section 3. A series of numerical assessments is presented as verification and validation cases in Section 5, and the results are discussed in Section 6. The conclusions of the present work are summarised in Section 7.

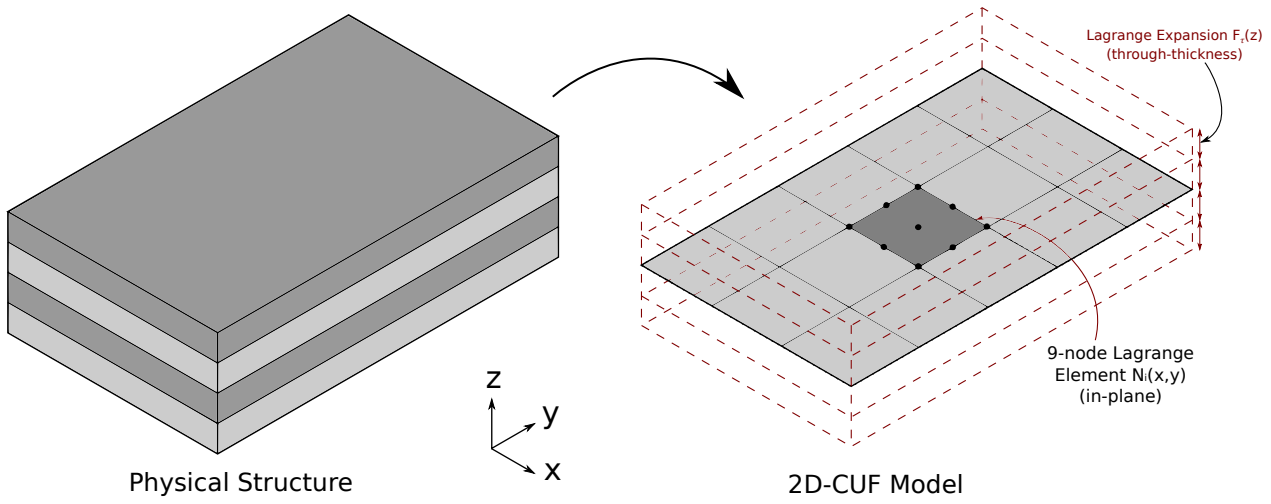


**Figure 1:** Layer-wise modeling of composite laminates in CUF.

## 2 Structural theories and FE formulation

Considering a multi-layered laminate, as shown in Fig. 1, the displacement field is described using layer-wise 2D CUF models in the following manner

$$\mathbf{u}(x,y,z) = F_\tau(z)\mathbf{u}_\tau(x,y), \tau = 1,2,\dots M \tag{1}$$

where $F_\tau(z)$ is the expansion function defining the kinematic approximation through the thickness of each layer of the laminate, $M$ refers to the number of terms in the expansion, and $\mathbf{u}_\tau(x,y)$ is the vector of generalized displacements. The choice of $F_\tau(z)$ and $M$ determines the model's structural theory and is a user input. The current work exploits Lagrange polynomials as expansion functions through the layer thickness. Such an approach, termed Lagrange-Expansion (LE) class in CUF terminology, results in a layer-wise structural model. Furthermore, LE models are purely based on displacement degrees of freedom (DOF). Further details of CUF structural models based on the LE class can be found in [19].

The 3D stress and strain fields are

$$\begin{aligned} \boldsymbol{\sigma} &= \{\sigma_{xx}, \sigma_{yy}, \sigma_{zz}, \sigma_{xy}, \sigma_{xz}, \sigma_{yz}\} \\ \boldsymbol{\varepsilon} &= \{\varepsilon_{xx}, \varepsilon_{yy}, \varepsilon_{zz}, \varepsilon_{xy}, \varepsilon_{xz}, \varepsilon_{yz}\} \end{aligned} \tag{2}$$

By considering the geometrically linear assumptions, the strain-displacement relation is given by

$$\boldsymbol{\varepsilon} = \mathbf{D}\mathbf{u} \tag{3}$$

where $\mathbf{u}$ is the displacement vector. The linear differential operator $\mathbf{D}$ is defined as

$$\mathbf{D} = \begin{bmatrix} \frac{\partial}{\partial x} & 0 & 0 \\ 0 & \frac{\partial}{\partial y} & 0 \\ 0 & 0 & \frac{\partial}{\partial z} \\ \frac{\partial}{\partial y} & \frac{\partial}{\partial x} & 0 \\ \frac{\partial}{\partial z} & 0 & \frac{\partial}{\partial x} \\ 0 & \frac{\partial}{\partial z} & \frac{\partial}{\partial y} \end{bmatrix}$$

The constitutive relation is

$$\boldsymbol{\sigma} = \mathbf{C}^{sec}\boldsymbol{\varepsilon} \tag{4}$$

where $\mathbf{C}^{sec}$ is the material secant stiffness matrix and is obtained from the constitutive model used in the analysis. The damaged stress state is represented by $\boldsymbol{\sigma}$. 2D FE, such as 4-node (Q4) or 9-node (Q9) quadrilateral elements with shape functions $N_i(x, y)$, are used to discretize the in-plane geometry, and in combination with 1D LE functions, lead to a 3D displacement field as follows

$$\mathbf{u}(x, y, z) = N_i(x, y)F_\tau(z)\mathbf{u}_{\tau i} \tag{5}$$

The semi-discrete balance of momentum is

$$\mathbf{M}\ddot{\mathbf{u}} = \mathbf{F}_{ext} - \mathbf{F}_{int} \tag{6}$$

where $\mathbf{M}$ is the mass matrix and $\ddot{\mathbf{u}}$ is the acceleration vector. The external and internal force vectors are denoted by $\mathbf{F}_{ext}$ and $\mathbf{F}_{int}$, respectively. The nonlinear system of equations is solved using explicit time integration techniques based on the central difference scheme. Further details on the development of an explicit nonlinear dynamics framework using CUF structural theories can be found in [24].

# 3 CODAM2 intralaminar compressive damage model

The CODAM2 material model implemented in the CUF framework has been previously described in [24] and is briefly recapitulated here for completeness. The basic formulation of the CODAM2 material model is based on a bilinear stress-strain response, with a linear post-peak softening. In this case, the fiber damage initiation, $F_1$, is determined using a maximum stress criterion as follows:

$$F_1 = \frac{\sigma_{11}}{X_C} \tag{7}$$

where $X_C$ is the fiber compressive strength, $\sigma_{11}$ is the stress in the fiber direction, and in general, subscripts $\{11, 22, 12\}$ indicate the in-plane stress and strain components in the principal material reference system. The damage initiation in the direction transverse to the fiber, i.e., matrix damage, is determined using the Hashin quadratic failure criterion [34] as

$$F_2 = \left(\frac{\sigma_{22}}{Y_C}\right)^2 + \left(\frac{\tau_{12}}{S_L}\right)^2 \tag{8}$$

where $Y_C$ and $S_L$ are the transverse compressive and in-plane shear strengths, respectively. The equivalent strain measures in the longitudinal and transverse directions are defined as

$$\varepsilon_1^{eq} = |\varepsilon_{11}| \tag{9}$$

$$\varepsilon_2^{eq} = \sqrt{(\gamma_{12})^2 + (\varepsilon_{22})^2} \tag{10}$$

where $\gamma_{12}$ is the in-plane shear strain component. The corresponding equivalent stress measures are given by

$$\sigma_1^{eq} = \sigma_{11} \tag{11}$$

$$\sigma_2^{eq} = \frac{\tau_{12}\gamma_{12} + \sigma_{22}\varepsilon_{22}}{\sqrt{(\gamma_{12})^2 + (\varepsilon_{22})^2}} \tag{12}$$

The damage initiation strains are computed as

$$\varepsilon_\alpha^i = \varepsilon_\alpha^{eq}|_{F_\alpha=1}, \quad \alpha = 1, 2 \tag{13}$$

where the subscripts 1 and 2 refer to fiber- and matrix-dominated damage, respectively. The strains at damage saturation are then evaluated as

$$\varepsilon_1^s = \frac{2g_1^f}{X_C} \quad and \quad \varepsilon_2^s = \frac{2g_2^f}{T} \tag{14}$$

where $g_\alpha^f$ is the fracture energy density, and $T = \sigma_2^{eq}|_{F_2=1}$ corresponds to the value of $\sigma_2^{eq}$ at matrix damage initiation. The spurious mesh dependency is mitigated by scaling the experimentally obtained fracture energy $G_\alpha^f$ with a characteristic length parameter of the element, following the crack-band theory [35], as shown below

$$g_\alpha^f = \frac{G_\alpha^f}{l^*}, \quad \alpha = 1, 2 \tag{15}$$

where $l^*$ is the characteristic element length. In the present work, this parameter is computed as $l^* = (V_{GP})^{\frac{1}{3}}$, where $V_{GP}$ is the volume associated with the given Gauss point of the element. The damage variables $\omega_1$ and $\omega_2$, which respectively quantify fiber and matrix damage, are computed as

$$\omega_\alpha = \left(\frac{\langle \varepsilon_\alpha^{eq} - \varepsilon_\alpha^i \rangle}{\varepsilon_\alpha^s - \varepsilon_\alpha^i}\right)\left(\frac{\varepsilon_\alpha^s}{\varepsilon_\alpha^{eq}}\right), \quad \alpha = 1, 2 \tag{16}$$

where $\langle\cdot\rangle$ denotes the Macaulay bracket. The damage variables are used to develop the 3D secant stiffness matrix, in the damaged state [31], as follows

$$\mathbf{C}^{dam} = \frac{1}{\Delta}\begin{bmatrix} (1-R_2\nu_{23}\nu_{32})R_1E_1 & (\nu_{21}+\nu_{23}\nu_{31})R_1R_2E_1 & (\nu_{31}+R_2\nu_{21}\nu_{32})R_1E_1 & 0 & 0 & 0 \\ & (1-R_1\nu_{31}\nu_{13})R_2E_2 & (\nu_{32}+R_1\nu_{31}\nu_{12})R_2E_2 & 0 & 0 & 0 \\ & & (1-R_1R_2\nu_{21}\nu_{12})E_3 & 0 & 0 & 0 \\ & & & \Delta R_1R_2G_{12} & 0 & 0 \\ & sym. & & & \Delta G_{23} & 0 \\ & & & & & \Delta G_{13} \end{bmatrix} \tag{17}$$

where $\Delta = 1 - R_2\nu_{23}\nu_{32} - R_1R_2\nu_{12}\nu_{21} - 2R_1R_2\nu_{31}\nu_{12}\nu_{23} - R_1\nu_{31}\nu_{13}$, and $R_\alpha$ is the stiffness reduction factor, defined as

$$R_\alpha = (1-\omega_\alpha), \qquad \alpha = 1,2 \tag{18}$$

The stress fields in the damaged state are then evaluated as

$$\boldsymbol{\sigma} = \mathbf{C}^{dam}\boldsymbol{\varepsilon} \tag{19}$$

Bilinear constitutive models with linear post-peak fiber softening may suffer in accurately evaluating the material behavior during compressive damage initiation and propagation. This is mainly due to the instabilities during the fiber failure initiation leading to fiber micro-buckling, and, eventually, kink-bands. Such a phenomenon is characterized by a sudden drop in the load-carrying capability, followed by a plateau of the stress response, and a simple linear post-peak softening curve is inadequate in modeling such a response under compressive loads [36, 37]. Given this, additional softening curves are implemented to improve the predictive capabilities of the material model [38], and such a process involves a modification of the damage evolution law (Eq. 16). Specifically, the current work considers a 'linear-brittle' post-peak softening curve to emulate the sudden drop and subsequent stable stress plateau. A series of such curves have been plotted in Fig. 2. The magnitude of the residual plateau stress is a percentage of the peak stress, and varying the percentage value leads to the family of curves shown in Fig. 2. The area under each curve (multiplied by the characteristic element length) remains constant and represents the fracture energy associated with the fiber constituent, which in the current work is 80 $kJ/m^2$ [39].

# 4 Verification

This section presents a series of single-element analyses to verify the implementation of the CODAM2 material model within the CUF framework, since such tests are a convenient method to verify each compressive failure mode's initiation and propagation independently. The material system used is the IM7/8552 carbon fiber

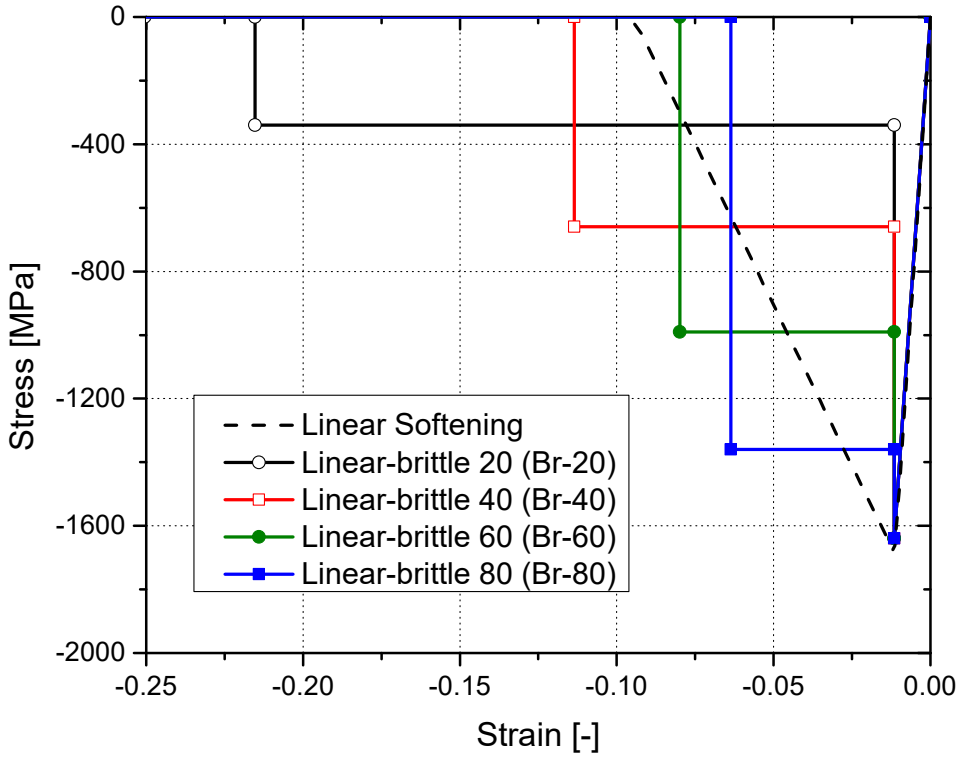


**Figure 2:** Linear and linear-brittle post-peak softening curves to model compressive fiber damage. The number indicates the percentage of the peak strength which remains as a residual stress plateau.

reinforced polymer (CFRP), with a nominal ply thickness of 0.125 mm, and whose elastic and strength properties are provided in Table 1. It is noted that the tensile strength and fracture toughness values are provided for completeness' sake and are not used in the numerical analyses, where only compressive loading is considered. In

**Table 1:** Material properties of IM7/8552 CFRP.

| $E_1$ [GPa] | $E_2$ [GPa] | $E_3$ [GPa] | $G_{12}$ [GPa] | $G_{13}$ [GPa] | $G_{23}$ [GPa] | $\nu_{12}$ | $\nu_{13}$ | $\nu_{23}$ |
|---|---|---|---|---|---|---|---|---|
| 150.0 | 11.0 | 11.0 | 5.8 | 5.8 | 2.9 | 0.34 | 0.34 | 0.48 |
| $X_T$ [MPa] | $X_C$ [MPa] | $Y_T$ [MPa] | $Y_C$ [MPa] | $S_{12}$ [MPa] | $G_1^T$ $[kJ/m^2]$ | $G_2^T$ $[kJ/m^2]$ | $G_1^C$ $[kJ/m^2]$ | $G_2^C$ $[kJ/m^2]$ |
| 2560.0 | 1690.0 | 73.0 | 250.0 | 90.0 | 120.0 | 2.6 | 80.0 | 4.2 |

the current verification tests, the structure is a unidirectional lamina modeled as a single element of size 1 mm $\times$ 1 mm and subjected to compression under uni-axial strain conditions. The in-plane discretization consists of one Q4 element. Each ply thickness kinematics is modeled via a single linear (LE1) Lagrange polynomial. The first assessment considers the compressive loading of the single element in the longitudinal direction, i.e., along the fiber (0°). The stress-strain response, predicted by the proposed approach, is shown in Fig. 3a. Similarly, the predicted response for the transverse compressive loading, i.e., perpendicular to the fiber (90°), is shown in Fig. 3b. The final assessment to verify the correct implementation of the CODAM2 material model in CUF-Explicit is the uniaxial compression of a single element quasi-isotropic $[90/45/0/-45]_{2s}$ laminate. Figure 4a shows the predicted stress-strain response, along with reference numerical results obtained via the CODAM2

implementation which is built into LS-DYNA [40], for comparison. Figure 4b presents the stress-strain curves extracted from the DIC measurements within the fracture process zone, obtained from compact compression tests of $[90/45/0/-45]_{4s}$ quasi-isotropic laminate [37]. The data corresponds to a 5 mm $\times$ 5 mm window, to account for the measured damage height of approximately 5 mm. This experimental data is subsequently used to develop the stress-strain input curve for the MAT81 macroscopic model (another built-in softening material model in LS-DYNA) and is overlaid in the plot, as explained in detail in [38], thereby forming the basis for the laminate-level LS-DYNA simulations presented in Section 5. The following observations are made based on the results of the single element studies:

1. The stress-strain response of single elements, loaded in compression parallel and transverse to the fiber, follows the bilinear path described by the CODAM2 material model with linear softening, as seen in Fig. 3. The peak stress in both cases corresponds to the input strength values of the fiber (1690 MPa) and matrix (250 MPa), as shown in Table 1 . Furthermore the area under the stress-strain curve matches the fracture energy provided as an input to the model (80 $kJ/m^2$ and 4.2 $kJ/m^2$ in the longitudinal and transverse directions, respectively).

2. The response of the 1 mm $\times$ 1 mm $[90/45/0/-45]_{2s}$ single element laminate, shown in Fig. 4, correlates well with numerical reference predictions obtained using LS-DYNA, in terms of laminate modulus, strength and fracture energy (area under the stress-strain curve).

3. The variation in the stress-strain response of the single element laminate, seen in Fig. 4, is attributed to the different structural modeling approaches used in the CUF and LS-DYNA analyses. The CUF analysis uses a combination of one Q4 and one LE1, while the LS-DYNA model uses a stacked 3D shell approach to model the single element laminate.

4. The stress-strain curves predicted by the numerical models with linear softening, shown in Fig. 4a, are qualitatively different when compared to the experimentally measured stress-strain response, shown in Fig. 4b, highlighting the limitations of bilinear damage models in describing laminate response under compressive loads. The CODAM2 implementation in CUF is extended to consider linear-brittle softening laws as shown in Fig. 2. The isotropic macroscopic model MAT81 uses user-defined stress-strain curves with arbitrary shapes as input at the laminate level.

The lamina-level single element studies constitute necessary verification tests and confirm the correct implementation of the CODAM2 material model for compressive damage initiation and progression in the CUF-Explicit framework.

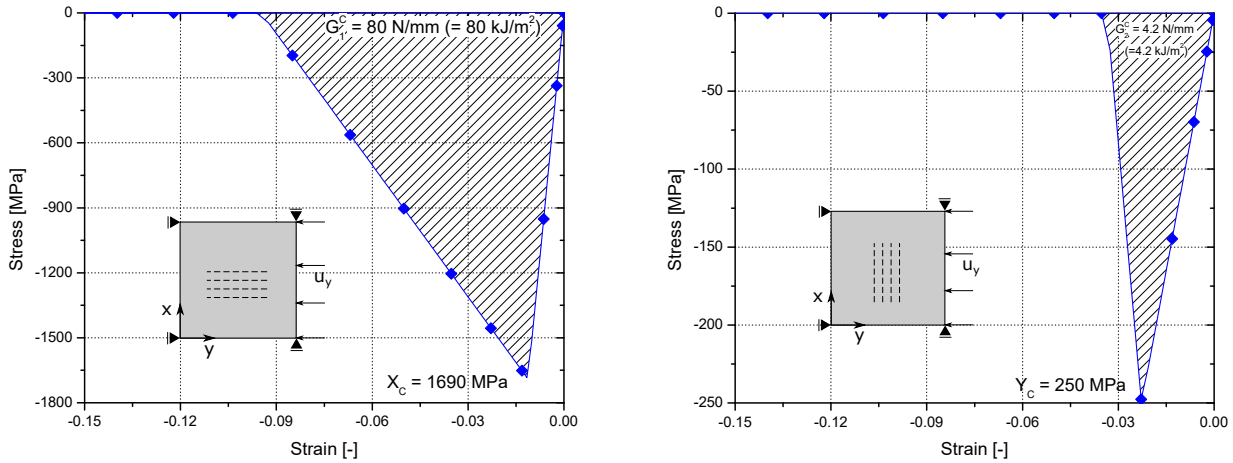


**(a)** Longitudinal loading (fiber) **(b)** Transverse loading (matrix)

**Figure 3:** Stress-strain curve of a 1 mm × 1 mm single element lamina loaded in compression under uni-axial strain conditions. Element loaded in (a) longitudinal (fiber) direction, and (b) transverse (matrix dominated) direction.

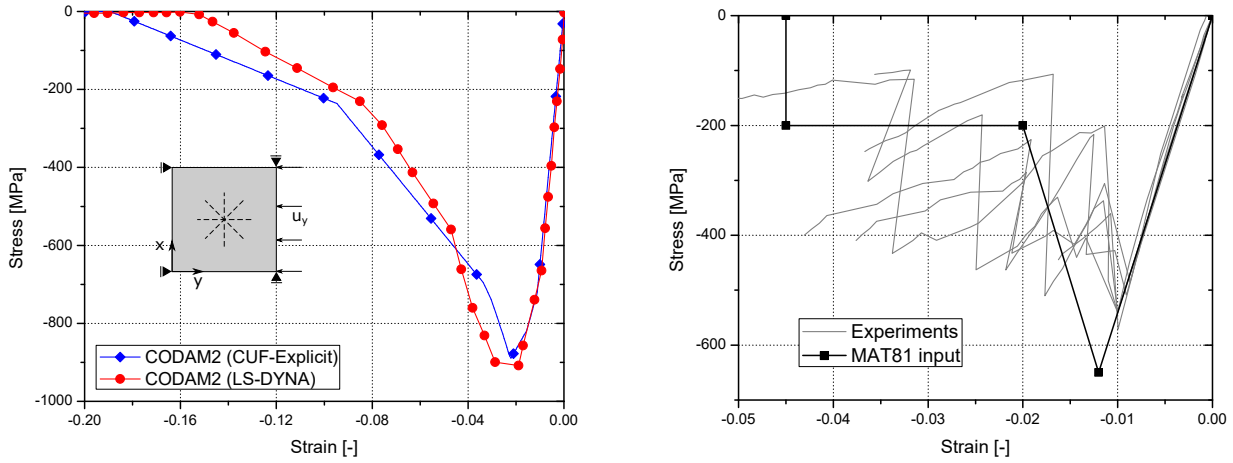


**(a)** **(b)**

**Figure 4:** Stress-strain curve of a 1 mm × 1 mm single element laminate loaded in compression. (a) Simulation of $[90/45/0/-45]_{2s}$ quasi-isotropic laminate under uni-axial strain, and (b) family of stress-strain curves derived from DIC measurements within the fracture process zone of a $[90/45/0/-45]_{4s}$ quasi-isotropic laminate [37], and input curve for the MAT81 macroscopic damage model [38].

# 5 Numerical examples

This section provides a series of numerical assessments as validation cases to demonstrate the capability of the proposed approach, based on CUF structural models, for the progressive damage analysis of composite laminates under compression. The numerical assessments include the influence of fiber post-peak softening curves, and the choice of through-thickness expansion functions, on the quality of results predicted by the CUF models. Reference numerical results are also provided for comparison, based on simulations performed in LS-DYNA using the macroscopic laminate-based MAT81 material model. As presented in detail in [38], quasi-isotropic laminates can be simulated by means of isotropic material models when delamination is negligible, and is hence applicable to the sublaminate-scaled, thin-ply laminates considered in the present work.

The material card MAT81 in LS-DYNA models elastoplastic materials with user-defined isotropic stress-strain curves to account for the coupling of damage and plasticity. This coupling is particularly useful to model residual deformations in composites subjected to impact or bending loads. In the present study, the macroscopic response of quasi-isotropic laminates subjected to compressive loadings is described by the stress-strain curve shown in Fig. 4b. Similar to the outlined linear-brittle softening in the CUF models shown in Fig. 2, the macroscopic response of the laminate under compression can be described by trilinear softening with stress plateau to account for fiber kinking.

## 5.1 Compact compression test

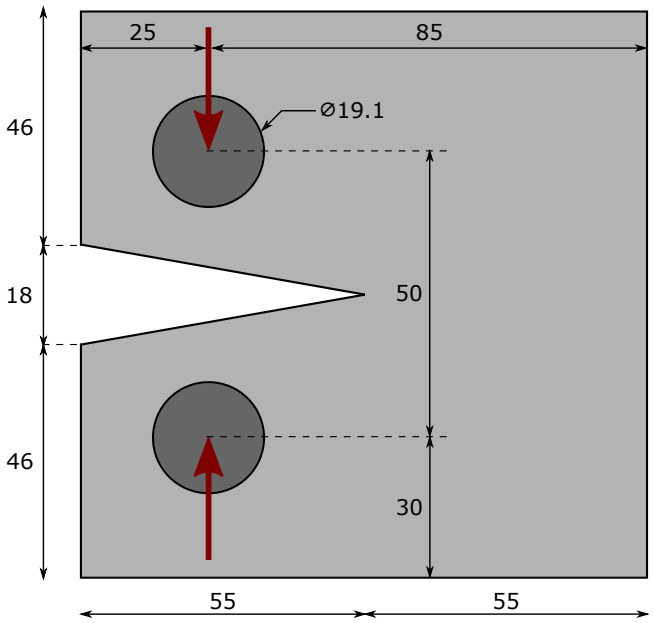


**Figure 5:** Schematic representation of the compact compression test specimen made of IM7/8552 CFRP with a $[90/45/0/-45]_{4s}$ quasi-isotropic layup (dimensions in mm).

The first numerical assessment is the simulation of the compact compression (CC) test of an IM7/8552 quasi-isotropic laminate with a $[90/45/0/-45]_{4s}$ stacking sequence. The laminate is loaded in compression

via prescribed displacements on the loading pins. A schematic representation of the CC specimen is shown in Fig. 5. The assessment is based on the work of Zobeiry et al. [37], which provides experimental data of the global force response as well as DIC analysis of the fracture process zone, presented in Fig. 4b. The CUF models consist of an in-plane mesh with 191 Q9 elements, see Fig. 6(a), which is obtained as the result of a mesh convergence study. A series of models are used with an increasing refinement in the thickness direction, using linear (LE1), quadratic (LE2), and cubic (LE3) expansion functions to describe the thickness of each ply of the laminate. Both linear and linear-brittle fiber softening options are used to investigate their influence on damage initiation and progression. The simulation of CC tests by the macroscopic (MAT81) model is achieved by the finite element discretization depicted in Fig. 6(b). The model consists of 4848 shell elements with an approximate element size of 1 mm $\times$ 1 mm in the expected fracture zone around the initial notch.

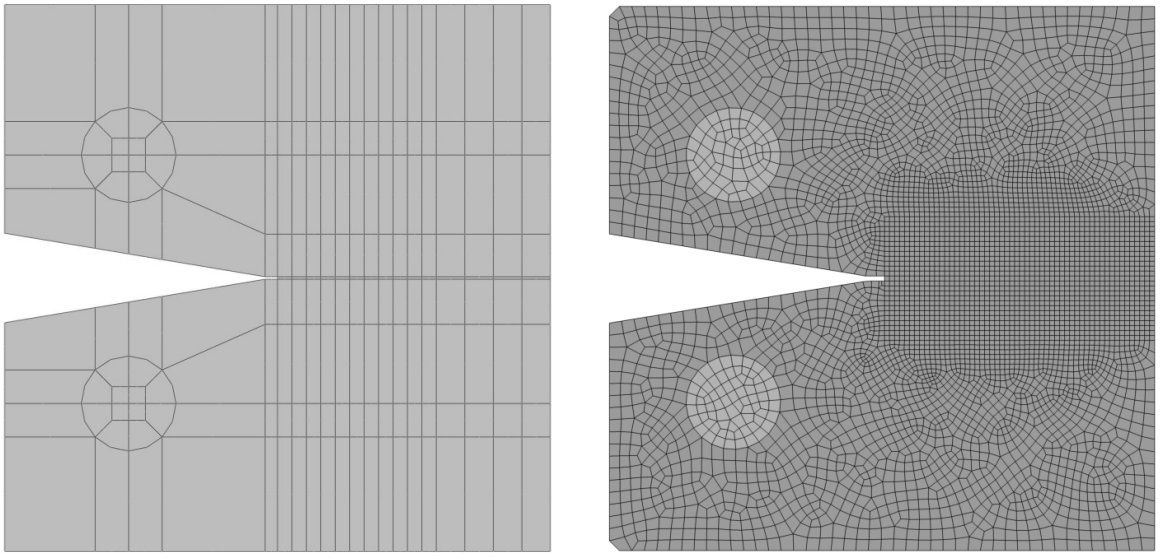


**Figure 6:** In-plane discretization of the compact compression specimen. (a) CUF-2D model with 191 Q9 elements, and (b) LS-DYNA model with 4848 shell elements.

The force-displacement response obtained from CUF simulations, considering LE1 and various softening options, is shown in Fig. 7. The linear-brittle model with 30% residual (plateau) stress, i.e., the Br–30 model, predicts a peak force that has the least error compared to the experimentally observed peak force (approximately 3.4%), and hence is selected for further analyses. The effect of higher-order through-thickness expansion functions in CUF is then studied, and the results are presented as force-displacement plots in Fig. 8, along with those obtained using a combination of higher-order expansions with a linear softening option. In each case, reference experimental data and numerical predictions based on the macroscopic MAT81 model, obtained from [37], are overlaid for comparison. A summary of the predicted peak force and the corresponding pin opening displacement (POD), according to the various numerical models, is listed in Table 2. The following observations are made:

1. The force-displacement response predicted by the CUF models is in good general agreement with the experimental curve, as seen in Fig. 7 and Fig. 8, in terms of predicted peak force as well as post-peak

softening behavior, thus validating the proposed framework.

2. The linear strain softening model in the fiber direction over-predicts the peak load by approximately 17% when compared to experimental observations, as seen in Fig. 7. Using a linear-brittle model, specifically the Br-30 curve, results in a more accurate prediction of the peak load, with an error of about 3.4%, as well as the subsequent global softening response due to progressive damage.

3. The peak force predicted by the CUF models with various post-peak softening curves, and their relative error with respect to experiments (see Table 2), indicate that the Br-30 softening curve is the most suitable option for the analysis of IM7/8852 composites using the proposed CUF approach.

4. The difference in the slope of the force-displacement curve in the linear regime, between the experimental and numerical approaches, may stem from limitations in replicating the actual experimental boundary conditions in the numerical models.

5. A non-negligible amount of noise is observed in the response, seen in Fig. 8, and is attributed to the inherent issues associated with the numerical modeling of compressive damage using explicit schemes, and the absence of numerical damping. The sudden loss of stiffness due to linear-brittle softening models may also contribute to such fluctuations in the response.

6. Considering the in-plane nature of the current problem, LE1 is sufficient to obtain solutions to the required accuracy. However, when significant interlaminar effects are present, such as delamination and laminate bending, LE1 may lead to oscillatory results, whereas higher-order (LE2 and LE3) thickness expansions provide a smooth and stable response, as observed in [25].

7. Similar to the CUF-LE1/Br-30 model, the macroscopic MAT81 model is able to predict the maximum force and post-peak response with reasonable accuracy, with an approximately 9% error in the peak force prediction compared to experiments. The macroscopic model predicts a smoother post-peak softening response due to the direct input of laminate properties in the numerical model. This is in contrast to the layer-wise approach of the CUF models, where the successive damage initiation and progression of individual plies lead to more abrupt changes in the stiffness, and could be a source of the observed oscillatory response.

## 5.2 Open-hole compression test

The next numerical assessment evaluates the performance of the proposed framework in the strength prediction of open-hole laminates subjected to compressive loads, schematically shown in Fig. 9. The analysis is based on the work of Lee and Soutis [41], providing reference to experimental data. Three scales of the open-hole specimen are studied, and their dimensions are listed in Table 3. The stacking sequence is $[45/90/-45/0]_{4s}$,

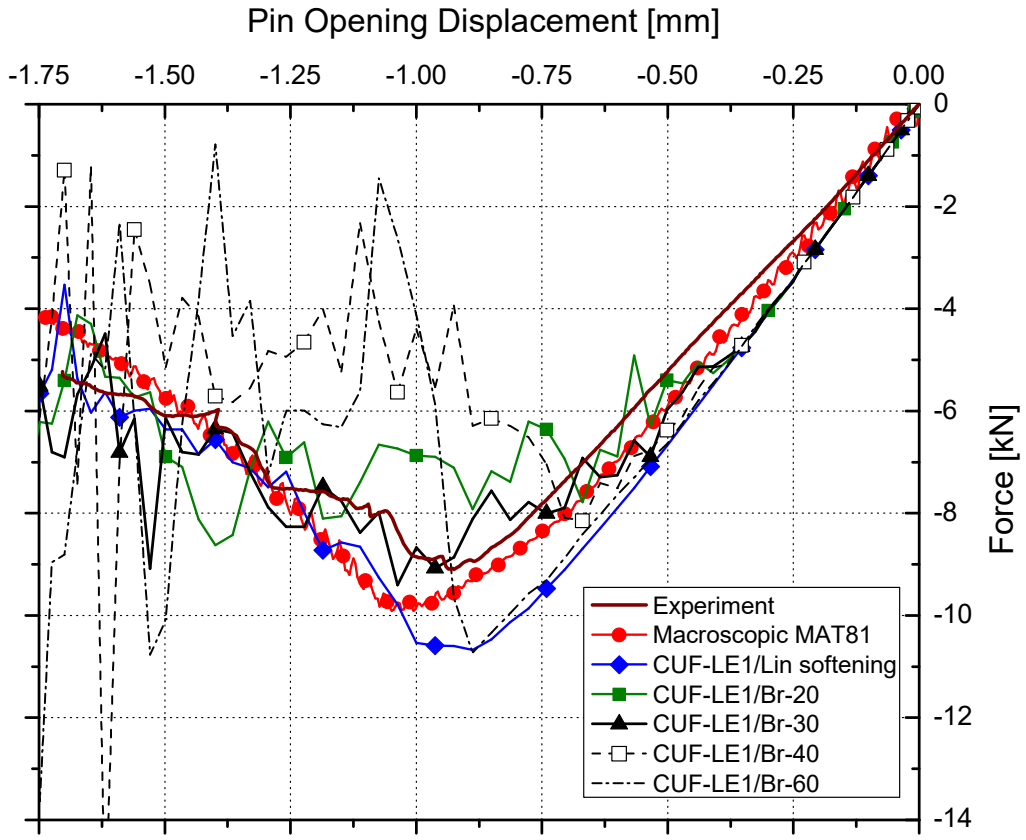


**Figure 7:** Force-displacement response of the IM7/8552 CFRP $[90/45/0/-45]_{4s}$ quasi-isotropic compact compression test specimen analyzed using various strain softening options in the fibre direction (LE1 used in each case). Experimental and MAT81 data obtained from [37].

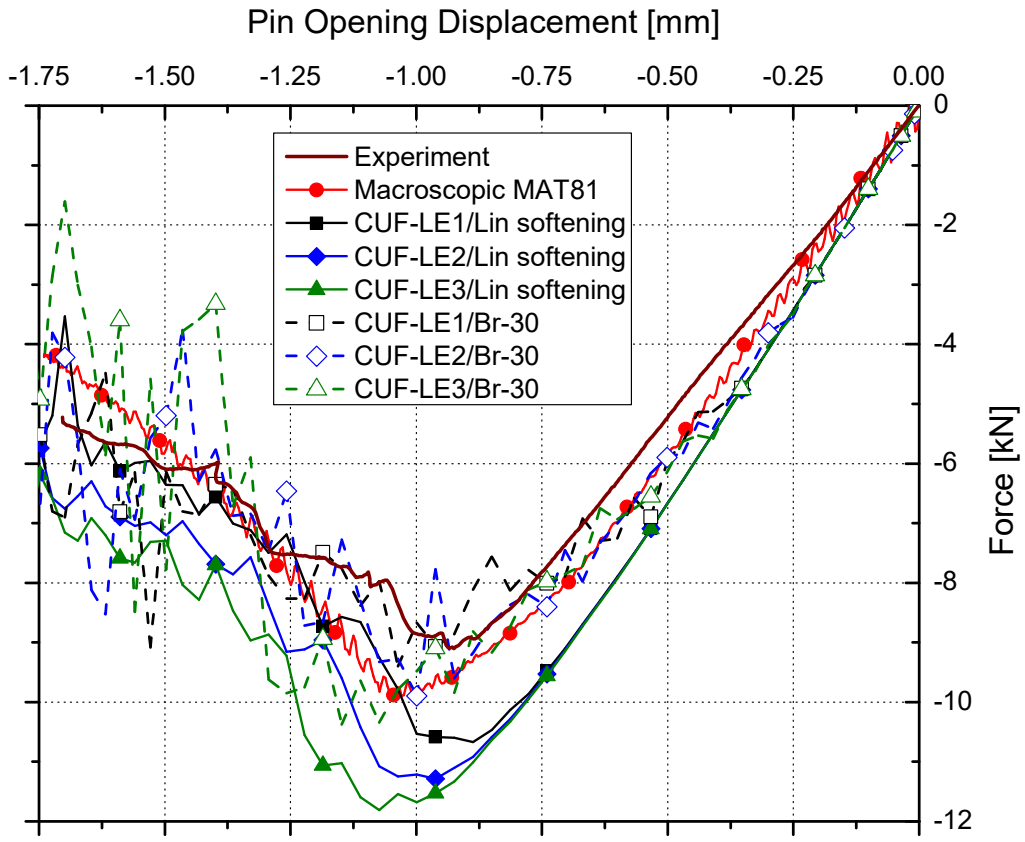


**Figure 8:** Force-displacement response of the IM7/8552 CFRP $[90/45/0/-45]_{4s}$ quasi-isotropic compact compression test specimen with increasing order of the ply thickness expansion function. Experimental and MAT81 data obtained from [37].

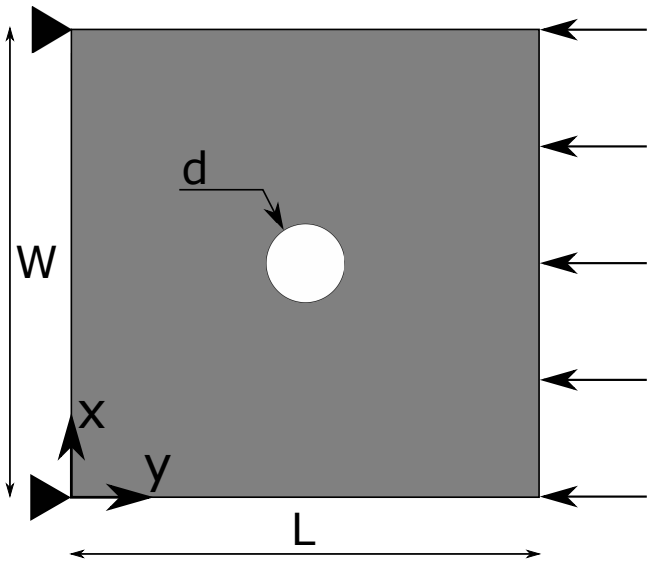


**Figure 9:** Schematic representation of the IM7/8552 CFRP open-hole compression specimen with a $[45/90/-45/0]_{4s}$ quasi-isotropic layup.

**Table 2:** Peak force of the IM7/8552 CFRP $[90/45/0/-45]_{4s}$ quasi-isotropic compact compression test specimen evaluated by experimental and numerical approaches.

| Approach | Peak Force [N] | Error* [%] | POD at peak force [mm] | Error* [%] |
|---|---|---|---|---|
| Experiment | 9092 | – | 0.932 | – |
| LS-DYNA (macroscopic MAT81) | 9912 | 9.0 | 1.005 | 7.8 |
| CUF-LE1/Lin softening | 10671 | 17.4 | 0.887 | -4.8 |
| CUF-LE2/Lin softening | 11283 | 24.1 | 0.962 | 3.2 |
| CUF-LE3/Lin softening | 11808 | 29.9 | 1.074 | 15.2 |
| CUF-LE1/Br-20 | 7782 | -14.4 | 0.669 | -28.2 |
| CUF-LE1/Br-40 | 8151 | -10.4 | 0.669 | -28.2 |
| CUF-LE1/Br-60 | 10728 | 18.0 | 0.887 | -4.8 |
| CUF-LE1/Br-30 | 9401 | 3.4 | 1.037 | 11.3 |
| CUF-LE2/Br-30 | 9897 | 8.9 | 0.999 | 7.2 |
| CUF-LE3/Br-30 | 10341 | 13.7 | 1.074 | 15.2 |

* Error computed with respect to experiments.

resulting in a quasi-isotropic composite laminate with a total thickness of 4 mm. The stacking sequence of the current case is slightly different from that of the previously described CC test, but involves the same damage modes due to the dispersed-ply nature of the laminate, with negligible amounts of delamination. A series of CUF layer-wise models have been developed, with a progressive refinement of the in-plane and through-thickness discretization. Both post-peak softening models, i.e., linear and linear-brittle softening curves, have been adopted in the analysis. Experimental data obtained from [41] and numerical predictions using LS-DYNA, based on the previously introduced macroscopic MAT81 approach, are also reported for comparison.

The first set of assessments investigates the influence of the linear and linear-brittle post-peak softening models on failure strength for the scale-1 specimen (see dimensions in Table 3). The failure strengths obtained using a linear softening curve are presented in Fig. 10, while the predictions obtained via the application of linear-brittle softening curves are presented in Fig. 11. The 48 Q9 in-plane mesh, used for the scale-1 model, is shown in Fig. 12(a). The scale-2 and scale-3 tests are then simulated, using CUF models with linear-brittle post-peak softening (Br-30), and the results are presented in Fig. 13. The in-plane mesh of the scale-2 and scale-3 CUF models consist of 128 Q9 and 256 Q9 elements, respectively, with LE1 over each ply. All the CUF models have an average element length of approximately 1.25 mm at the hole boundary. For the case of the MAT81 analysis in LS-DYNA, the scale-1 laminate is discretized using 1202 shell elements, see Fig. 12(b), with an approximate element size of 1 mm $\times$ 1 mm. Details of the various CUF models, such as the discretization used and analysis (wall) time, are listed in Table 4. The following comments are made:

1. The use of linear post-peak fiber softening leads to an approximately 60% overestimation of the predicted failure strength in open-hole laminates, as seen in Fig. 10. The error remains constant with the progressive refinement of the in-plane and through-thickness discretization.

2. Using linear-brittle softening models leads to significant improvements in the results' quality, as seen in Fig. 11. In particular, the Br-30 model predicts a failure strength which is in excellent agreement with experimental data (error below 1.5%), and remains constant with progressive refinement of the mesh.

3. As seen in Fig. 13, the failure strength predictions of the CUF models at all three scales correlate very well with experimental results, with a maximum error below 4%. Furthermore, the size-effect, which is experimentally observed by scaling the specimen dimensions, is also evident in the CUF predictions.

4. The macroscopic MAT81 model is able to predict the strength at all three scales with good accuracy with a maximum error of 7% compared to experiments. It should be noted that this only requires a coarse discretization of 1202 elements (for the scale-1 specimen). The CUF modeling approach requires even fewer elements, leading to highly efficient simulation of damage progression in composite laminates.

5. A direct comparison of the computation time between the CUF-Explicit and the LS-DYNA analyses is not possible, since the layer-wise CUF models use the CODAM2 material model, whereas the LS-DYNA models are based on the isotropic macroscopic MAT81 approach.

**Table 3:** Dimensions of the three scales considered for the open-hole compression tests.

| Scale | Gauge length L [mm] | Gauge width W [mm] | Diameter d [mm] |
|---|---|---|---|
| scale - 1 | 32 | 32 | 6.35 |
| scale - 2 | 64 | 64 | 12.70 |
| scale - 3 | 128 | 128 | 25.40 |

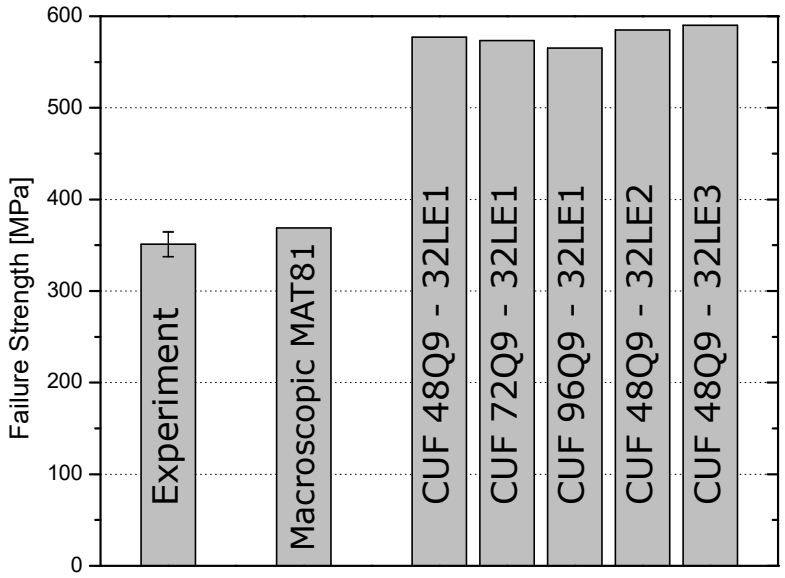


**Figure 10:** Predicted failure strength of the $[45/90/-45/0]_{4s}$ quasi-isotropic open-hole compression specimen based on various CUF models with linear post-peak softening (scale-1 test). Experimental results are from [41].

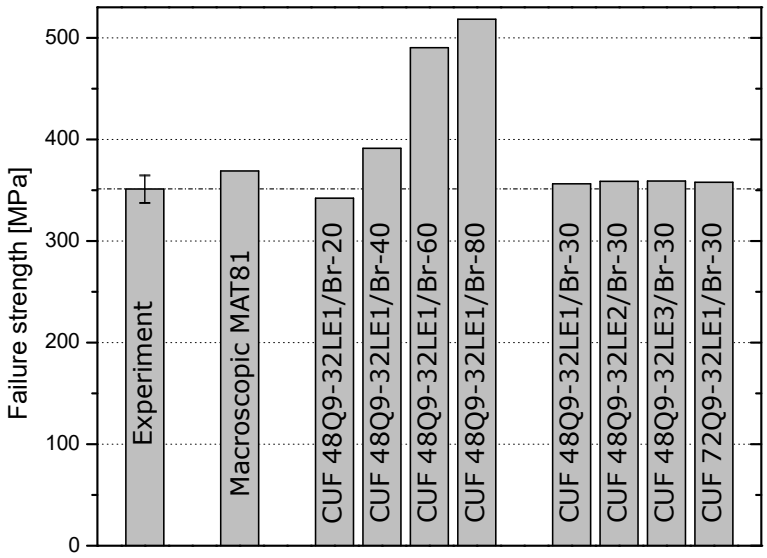


**Figure 11:** Predicted failure strength of the $[45/90/-45/0]_{4s}$ quasi-isotropic open-hole compression specimen based on various CUF models with linear-brittle post-peak softening (scale-1 test). Experimental results are from [41].

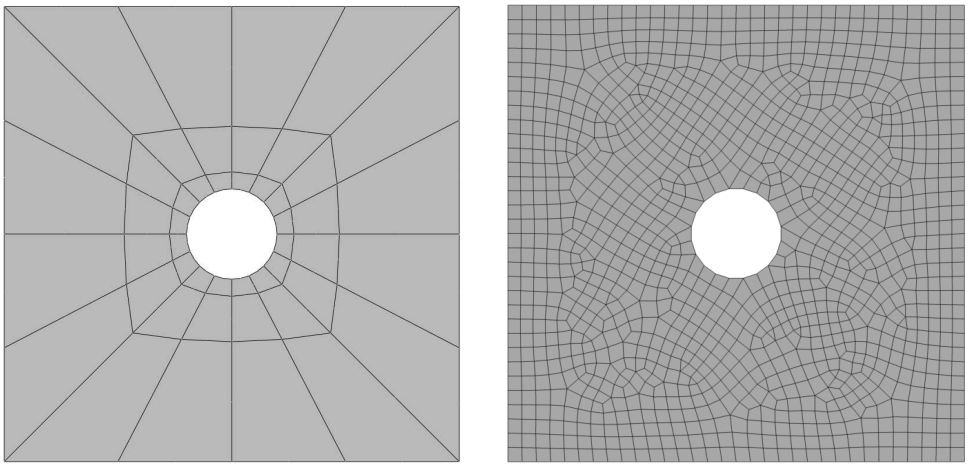


**Figure 12:** In-plane discretization of the scale-1 open-hole compression. (a) CUF-2D model with 48 Q9 elements, and (b) LS-DYNA model with 1202 shell elements.

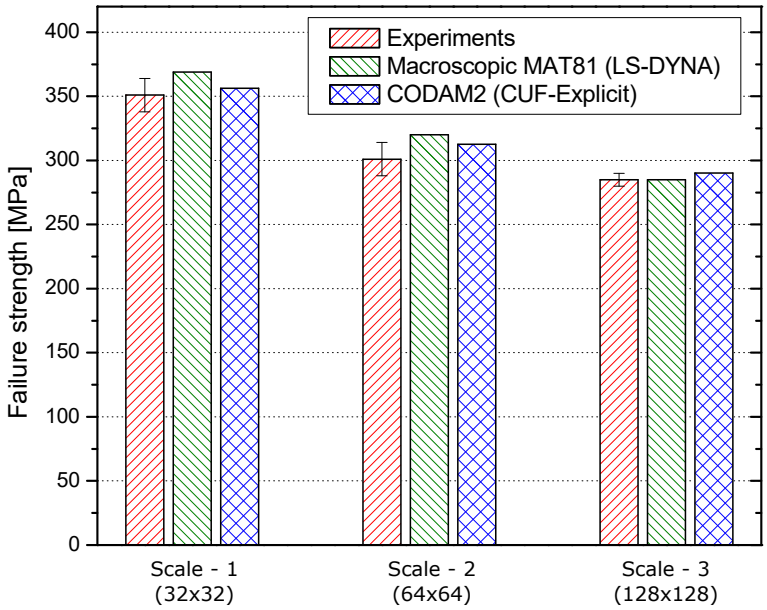


**Figure 13:** Predicted failure strengths of the the $[45/90/-45/0]_{4s}$ quasi-isotropic open-hole compression specimen for all the scales by CUF models with linear brittle (Br-30) post-peak softening. Experimental results from [41].

**Table 4:** Model information for the $[45/90/-45/0]_{4s}$ quasi-isotropic open-hole compression test.

| Model | Discretization of the open-hole specimen | DOF | Analysis Time* [hh:mm:ss] |
|---|---|---|---|
| | **scale-1 test (L = 32 mm, W = 32 mm)** | | |
| CUF 48Q9 - 32LE1 | 48 Q9 elements in-plane (1 LE1/ply) | 22,176 | 00:29:34 |
| CUF 48Q9 - 32LE2 | 48 Q9 elements in-plane (1 LE2/ply) | 43,680 | 01:20:23 |
| CUF 48Q9 - 32LE3 | 48 Q9 elements in-plane (1 LE3/ply) | 65,184 | 02:51:20 |
| CUF 72Q9 - 32LE1 | 72 Q9 elements in-plane (1 LE1/ply) | 33,264 | 00:46:51 |
| | **scale-2 test (L = 64 mm, W = 64 mm)** | | |
| CUF 128Q9 - 32LE1 | 128 Q9 elements in-plane (1 LE1/ply) | 57,024 | 01:49:03 |
| | **scale-3 test (L = 128 mm, W = 128 mm)** | | |
| CUF 256Q9 - 32LE1 | 256 Q9 elements in-plane (1 LE1/ply) | 114,048 | 03:09:29 |

* The reported run-times are based on analyses performed on a desktop computer using 6 cores

### 5.3 Center-notched compression test

The final numerical assessment extends the failure strength prediction evaluation to the case of center-notched laminates under compressive loads. The assessment is based on the works of Xu et al. [42], where a series of 4 mm thick $[45/90/-45/0]_{4s}$ quasi-isotropic IM7/8552 laminates of varying dimensions were experimentally investigated. The scale-8 laminate (see Ref. [42]) is analyzed in the present work, and the gauge section is modeled as shown schematically in Fig. 14. Based on the previous open-hole compression analysis observations, the current study directly considers LE1 for each ply, and the Br-30 fiber softening model to account for damage progression. The in-plane geometry is discretized with three successively refined meshes using Q9 elements. For comparison, the macroscopic MAT81 model in LS-DYNA consists of about 20,000 shell elements with an approximate size of 1 mm $\times$ 1 mm. The force-displacement response of the center-notched laminate, obtained from the CUF models and experimental data, are overlaid in Fig. 15. The experimentally observed and numerically predicted peak strength values are tabulated in Table 5. The contour plot of the damage state, at and immediately after the peak load, is shown in Fig. 16. The following comments are made:

1. The modeling options leading to accurate strength predictions of open-hole laminates remain suitable for analyzing center-notched laminates in compression, as seen in Fig. 15. The peak strength predicted by the CUF model is in perfect agreement with experimental data (0% error), as seen in Table 5.

2. Similarly, the results obtained from the macroscopic MAT81 analysis are consistent with previous findings in the simulation of CC and OHC tests, and are in good agreement with experimental data. The peak strength prediction of 248 MPa is around 5% higher than the experimentally measured strength of the

scale-8 specimen.

3. The fiber damage morphology predicted by the CUF model correlates well with that of the macroscopic MAT81 model in LS-DYNA, see Fig. 16, and the numerical predictions are in line with experimental observations, see Fig. 3b of Ref. [42], where cracks initiate at the notch tip, and propagate along the notch plane. Furthermore, the CUF implementation of CODAM2 allows for the determination of both fiber and matrix damage, whereas the macroscopic MAT81 model in LS-DYNA computes a single isotropic damage variable.

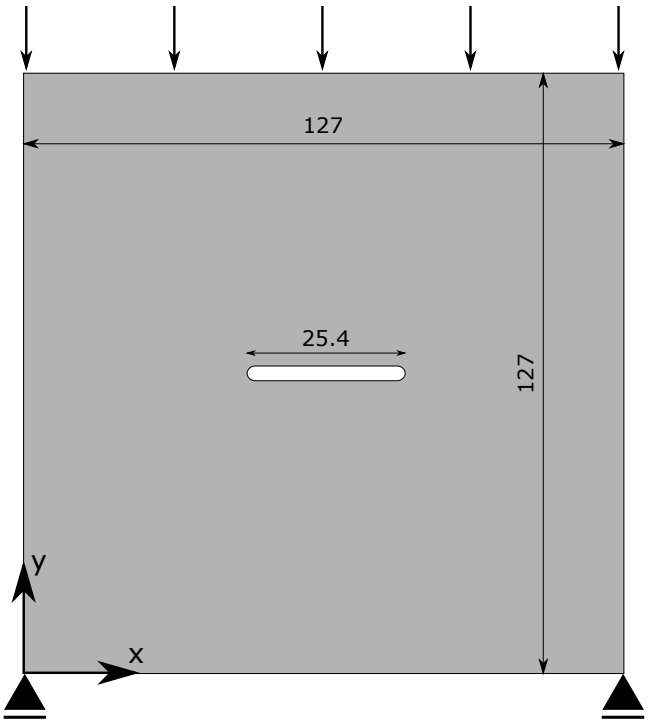


**Figure 14:** Schematic representation of the $[45/90/-45/0]_{4s}$ quasi-isotropic center-notched compression specimen (dimensions in mm).

**Table 5:** Peak force of the the $[45/90/-45/0]_{4s}$ quasi-isotropic center-notched compression specimen evaluated by experimental and numerical approaches.

| Approach | Peak Strength [MPa] | Error w.r.t experiments [%] |
|---|---|---|
| Experiment [42] | 235.0(0.4*) | – |
| LS-DYNA (MAT81) | 248.0 | 5 |
| CUF 108Q9-32LE1/Br-30 | 235.0 | 0 |

* Coefficient of variation [%]

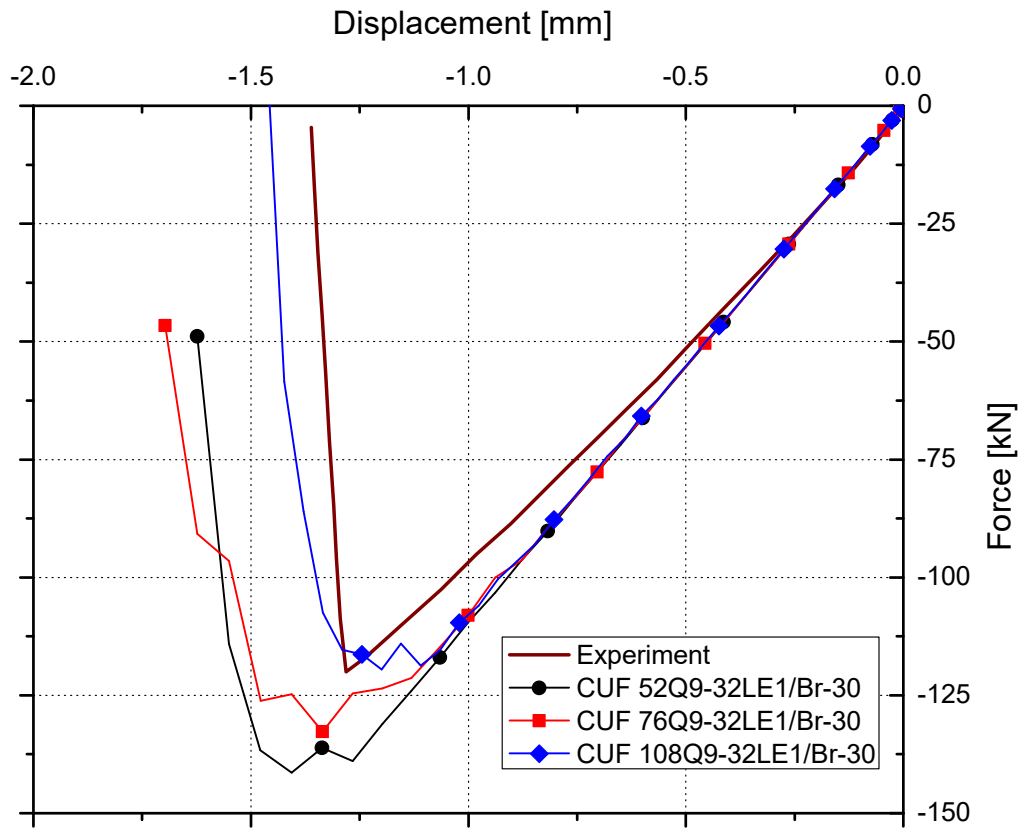


**Figure 15:** Force-displacement response of the $[45/90/-45/0]_{4s}$ quasi-isotropic center-notched compression specimen. Experimental results from [42].

# 6 Discussion

The first set of numerical assessments consists of single element studies to verify the correct implementation of the CODAM2 model for compressive damage within the CUF-explicit numerical framework. A 1mm $\times$ 1mm single element lamina is loaded in compression along the fiber direction, leading to fiber-dominated damage, and the resulting stress-strain response is shown in Fig. 3a. The predicted peak stress corresponds to the input fiber strength value $X_C = 1690$ MPa, and the area under the curve (multiplied by the element length of 1 mm) corresponds to the fiber fracture energy $G_1^C = 80\ kJ/m^2$. The choice of fiber fracture energy has significant consequences on damage progression and failure. However, investigating such an influence is beyond the scope of the present work, and the predictive capabilities of the proposed numerical framework is assessed by considering a fixed value of the fracture energy. Next, the same single element lamina is loaded in compression transverse to the fiber, leading to matrix-dominated damage, and the stress-strain response obtained is plotted in Fig. 3b. As in the case of fiber loading, the predicted peak stress is in agreement with the matrix strength $Y_C = 250$ MPa, which is an input parameter. The area under the stress-strain curve corresponds to the matrix fracture energy $G_2^C = 4.2\ kJ/m^2$. The value of $G_2^C$ was chosen to ensure that matrix cracks lead to brittle failure under transverse compression. The final single element assessment considers a $[90/45/0/-45]_{2s}$ laminate loaded in uniaxial compression. As seen in Fig. 4, the predicted stress-strain response of the single element laminate is in

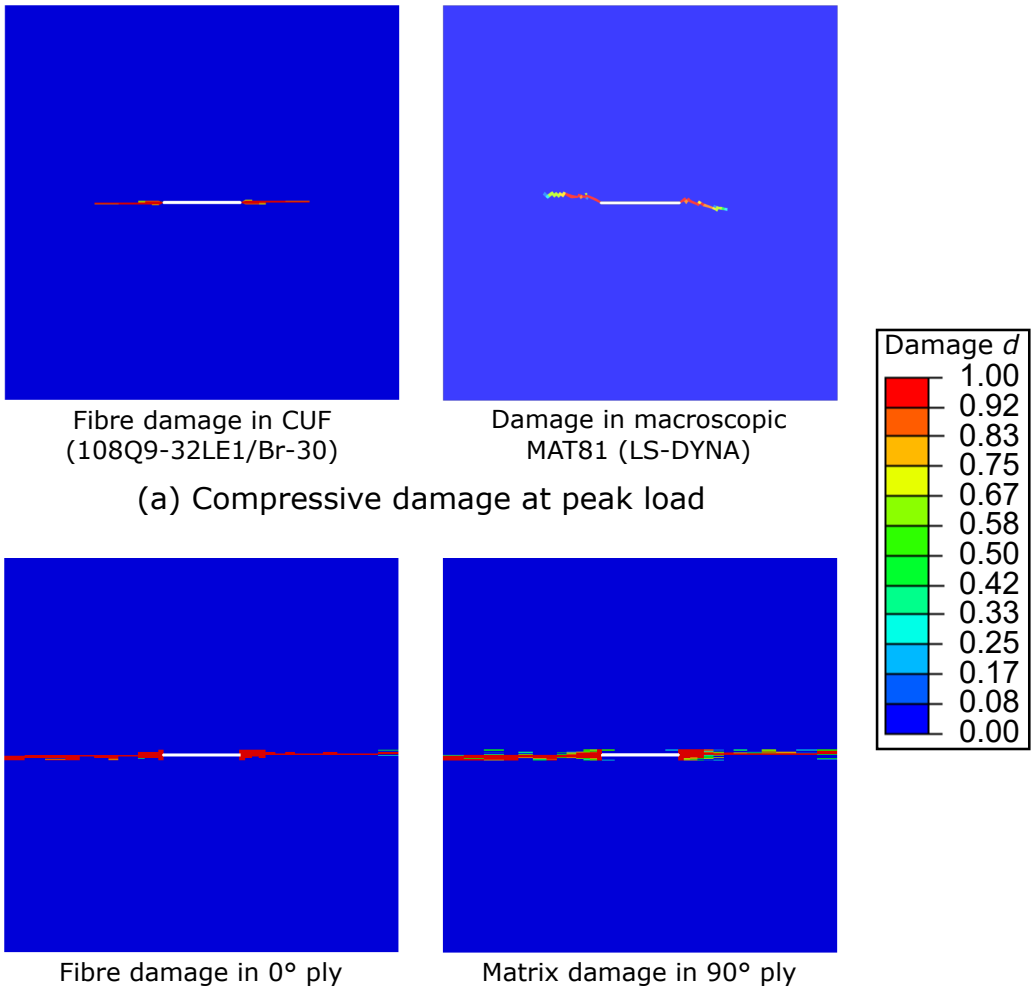


**Figure 16:** Damage state in the $[45/90/-45/0]_{4s}$ quasi-isotropic center-notched compression specimen. (a) Compressive damage predicted by CUF and LS-DYNA models at peak load, and (b) Fiber (0° ply) and matrix (90° ply) damage predicted by the CUF 108Q9-32LE1/Br-30 model immediately after the peak load.

good agreement with numerical reference predictions obtained from the built-in CODAM2 version in LS-DYNA. The obtained results confirm the correct implementation of the CODAM2 material model in the CUF-Explicit framework, and the numerical platform can subsequently be used for the analysis of laminates subjected to compression.

A series of numerical assessments are then presented as validation cases, where the predictive capabilities of the CUF models are evaluated with respect to experiments. The results are also compared with LS-DYNA models based on the macroscopic MAT81 model which uses laminate-level properties as input data. The first numerical assessment is the compact compression test of a $[90/45/0/-45]_{4s}$ quasi-isotropic laminate. The first study investigates the influence of the post-peak fiber softening curve used in the model, considering LE1. The obtained force-displacement curves are presented in Fig. 7. It is seen that the use of linear softening curves leads to an approximately 17% over-prediction of the peak load carrying capacity, compared to experiments, since the effects of fiber micro-buckling and kinking are not taken into account in such models. Such phenomenological effects are accounted for in the linear-brittle fiber softening model, and multiple such curves are considered to calibrate the magnitude of the residual (plateau) stress after the load drop due to brittle failure (see Fig. 2). Using the linear-brittle model with 30% residual stress in the fiber direction, i.e. the Br-30 model, results in an accurate prediction of the peak forces, with an error of about 3.4% compared to experiments, as well as a better evaluation of the global post-peak softening behavior. Larger magnitudes of the residual stress, such as Br-40 and Br-60, lead to inaccurate and highly oscillatory results. This observed response is attributed to the sudden drop of larger stress magnitudes and loss of stiffness (see Fig. 2) upon complete failure of the material at the evaluated Gauss point, for linear-brittle models with higher residual stresses. The next set of assessments studies the influence of the ply thickness expansion function on the laminate's global response. It is seen from Fig. 8 that higher-order expansions such as LE2 and LE3 do not lead to significant improvements in the quality of the results, compared to LE1. This is due to the fact that delamination is negligible in fracture tests of dispersed quasi-isotropic laminates and intralaminar damage is therefore the primary factor that influences global structural behavior. However, higher-order thickness expansions are needed when interlaminar effects become more important, as in the case of delamination-dominated fracture tests of ply-scaled (blocked) laminates, or when the laminate undergoes bending deformation, based on the findings reported in [25].

An advantage of using Q9 elements to discretize the in-plane geometry is a relaxation of element aspect-ratio and size constraints, as observed in Fig. 6(a), where the global structure is meshed with very few elements. This is in contrast to standard linear finite elements, see Fig. 6(b), where a higher number of elements are required. The second-order interpolation functions used in the Q9 elements allow for the accurate evaluation of strain and stress fields with a coarser discretization, leading to computationally-efficient structural models. Only the region ahead of the crack-tip is finely meshed, with an average element dimension of $0.5 \times 3$ mm, and is due to element size requirements for material models based on continuum damage mechanics. The occurrence of numerical oscillations in the results suggests applying numerical damping techniques as a scope for future

works.

The second numerical assessment is the compressive strength prediction of open-hole $[90/45/0/-45]_{4s}$ quasi-isotropic laminates. The first study investigated the scale-1 open-hole compression specimen, where fiber damage progression is modeled using a linear softening curve. Similar to the case of the CC test, the limitations of linear softening curves result in highly over-predicted compressive strengths, see Fig. 10, with an error of about 60% compared to experimental observations. The error remains constant with further mesh refinements of the structural model, indicating convergence of the solution, and hence stems from the limitations of linear fiber softening models. Using linear-brittle softening models, specifically the Br-30 curve, results in accurate strength predictions, with an error of about 1.5% compared to experimental results, as seen in Fig. 11. In the second part of the assessment, three scales of the open-hole specimen were analyzed using the current approach, and the predicted strength in each case was in good agreement with reference experimental and numerical data, with a maximum error under 4% compared to experiments. Furthermore, a size-effect was predicted with increasing the composite laminate scale, which is consistent with trends observed in experimental data, as seen in Fig. 13. The analysis of different scales required the use of modified meshes with an increase in the computational cost. In the case of tension loading [24], on the other hand, the same meshes can be used for different scales, i.e., lower computational costs are needed for larger scales.

The final compressive strength assessment considers the center-notched specimen, shown schematically in Fig. 14. Based on the results of previous validation cases, the Br-30 linear-brittle curve was directly utilized to develop the CUF model, in combination with LE1. From Fig. 15, it is seen that the CUF 108 Q9 - 32 LE1 model prediction of the force-displacement response and peak loads are in good agreement with experimental curves, and the predicted peak strength is in perfect agreement with experimental observations, see Table 5. The obtained results confirm the suitability of the Br-30 linear-brittle fiber softening curve for compressive damage analysis of IM7/8552 composite laminates.

The comparison of the results from experiments and the explicit CUF implementation of CODAM2 to predictions obtained from macroscopic MAT81 show that the structural response of quasi-isotropic dispersed laminates can also be represented at the laminate level. Simulations of open-hole compression and center-notch compression tests yield reasonable strength predictions with errors of less than 10% compared to experiments. Such macroscopic material modeling is a practical alternative to mesoscopic models since the characterization of ply-based properties can be challenging, in particular strength and fracture energy values. However, these macroscopic material models are limited to quasi-isotropic layups.

# 7 Conclusion

The present work combines the CODAM2 material model with higher-order 2D structural theories obtained via the Carrera Unified Formulation to develop a numerical framework for the progressive damage analysis

of unidirectional fiber-reinforced composites loaded in compression. The CODAM2 model is applied at the ply-level, where damage initiation is determined using Hashin's failure criteria, and damage evolution and propagation is governed using a smeared crack approach. The CUF-based structural models are based on higher-order plate theories, where each ply of the laminate is individually modeled using Lagrange polynomials and resulting in a layer-wise model. A series of numerical assessments, based on IM7/8552 composite laminates, have been presented to verify and validate the proposed framework. The initial verification of the model implementation was carried out via a series of single elements tests. The next set of assessments was the compact compression test of quasi-isotropic laminates. The final assessment was the failure strength prediction of notched quasi-isotropic laminates, such as open-hole and center-notched specimens under compression. Multiple post-peak softening options were used in the numerical models to account for the effects of fiber micro-buckling and kinking. The use of linear-brittle softening curves was advantageous compared to simple linear softening laws regarding the accuracy of results. The application of linear-brittle curves resulted in a more accurate prediction of peak load-carrying capacity and post-peak global response for the compact compression test case compared to the use of linear softening models. Similarly, the predicted compressive failure strengths of the open-hole and center-notched laminates were in excellent agreement with experimental data for linear-brittle models. At the same time, the use of linear softening curves significantly over-predicted the compressive strength. It is demonstrated that the combination of higher-order 2D structural models based on CUF and the CODAM2 material model constitutes an accurate numerical simulation platform for the progressive damage analysis of fiber-reinforced composites subjected to compression. Compared to tensile loadings, the compressive case required higher computational costs.

The present work aimed to develop accurate compressive damage modeling capabilities at the mesoscopic level, based on layer-wise structural models. This development constitutes a building block approach toward the high-fidelity analysis of more complex structural problems involving compressive damage. Future works aim to extend the numerical framework's capabilities towards compression-after-impact (CAI) analysis of laminated composites.

## Acknowledgements

This research work has been carried out within the project ICONIC (Improving the Crashworthiness of Composite Transportation Structures), funded by the European Union Horizon 2020 Research and Innovation program under the Marie Skłodowska-Curie Grant agreement No. 721256, and the Joint Project for the Internationalization of Research // Polito MUL2 — University of British Columbia. Computational resources were provided by HPC @ POLITO (http://www.hpc.polito.it).

# References


[1] Q Sun, G Zhou, H Guo, Z Meng, Z Chen, H Liu, H Kang, and X Su. Failure mechanisms of cross-ply carbon fiber reinforced polymer laminates under longitudinal compression with experimental and computational analyses. *Composites Part B: Engineering*, 167:147–160, 2019.

[2] MR Wisnom. The effect of fibre misalignment on the compressive strength of unidirectional carbon fibre/epoxy. *Composites*, 21(5):403–407, 1990.

[3] SH Lee and AM Waas. Compressive response and failure of fiber reinforced unidirectional composites. *International Journal of Fracture*, 100(3):275–306, 1999.

[4] Y Yuan, K Niu, and Z Zhang. Compressive damage mode manipulation of fiber-reinforced polymer composites. *Engineering Fracture Mechanics*, 223:106799, 2020.

[5] X Chen, X Sun, B Wang, J Gu, P Zou, Y Chai, and J Yang. An improved longitudinal failure criterion for ud composites based on kinking model. *Mechanics of Advanced Materials and Structures*, In Press.

[6] CR Schultheisz and AM Waas. Compressive failure of composites, part i: testing and micromechanical theories. *Progress in Aerospace Sciences*, 32(1):1–42, 1996.

[7] AM Waas and CR Schultheisz. Compressive failure of composites, part ii: experimental studies. *Progress in Aerospace Sciences*, 32(1):43–78, 1996.

[8] EV Iarve, KH Hoos, Y Nikishkov, and A Makeev. Discrete damage modeling of static bearing failure in laminated composites. *Composites Part A: Applied Science and Manufacturing*, 108:30–40, 2018.

[9] S Rivallant, C Bouvet, and N Hongkarnjanakul. Failure analysis of cfrp laminates subjected to compression after impact: Fe simulation using discrete interface elements. *Composites Part A: Applied Science and Manufacturing*, 55:83–93, 2013.

[10] ZC Su, TE Tay, M Ridha, and BY Chen. Progressive damage modeling of open-hole composite laminates under compression. *Composite Structures*, 122:507–517, 2015.

[11] MR Abir, TE Tay, M Ridha, and HP Lee. Modelling damage growth in composites subjected to impact and compression after impact. *Composite Structures*, 168:13–25, 2017.

[12] A Riccio, A Sellitto, S Saputo, A Russo, M Zarrelli, and V Lopresto. Modelling the damage evolution in notched omega stiffened composite panels under compression. *Composites Part B: Engineering*, 126:60–71, 2017.

[13] XC Sun and SR Hallett. Barely visible impact damage in scaled composite laminates: Experiments and numerical simulations. *International Journal of Impact Engineering*, 109:178–195, 2017.

[14] M Akterskaia, E Jansen, SR Hallett, PM Weaver, and R Rolfes. Progressive failure analysis using global-local coupling including intralaminar failure and debonding. *AIAA Journal*, pages 3078–3089, 2019.

[15] E Pietropaoli and A Riccio. A global/local finite element approach for predicting interlaminar and intralaminar damage evolution in composite stiffened panels under compressive load. *Applied Composite Materials*, 18(2):113–125, 2011.

[16] J Chen, EV Morozov, and K Shankar. Simulating progressive failure of composite laminates including inply and delamination damage effects. *Composites Part A: Applied Science and Manufacturing*, 61:185–200, 2014.

[17] SI Thorsson, AM Waas, and M Rassaian. Low-velocity impact predictions of composite laminates using a continuum shell based modeling approach part b: Bvid impact and compression after impact. *International Journal of Solids and Structures*, 155:201–212, 2018.

[18] J Reiner, T Feser, D Schueler, M Waimer, and R Vaziri. Comparison of two progressive damage models for studying the notched behavior of composite laminates under tension. *Composite Structures*, 207:385–396, 2019.

[19] E Carrera, M Cinefra, M Petrolo, and E Zappino. *Finite element analysis of structures through unified formulation*. John Wiley & Sons, 2014.

[20] AG de Miguel, I Kaleel, MH Nagaraj, A Pagani, M Petrolo, and E Carrera. Accurate evaluation of failure indices of composite layered structures via various fe models. *Composites Science and Technology*, 167:174–189, 2018.

[21] M Petrolo, MH Nagaraj, I Kaleel, and E Carrera. A global-local approach for the elastoplastic analysis of compact and thin-walled structures via refined models. *Computers & Structures*, 206:54–65, 2018.

[22] MH Nagaraj, I Kaleel, E Carrera, and M Petrolo. Contact analysis of laminated structures including transverse shear and stretching. *European Journal of Mechanics-A/Solids*, page 103899, 2019.

[23] MH Nagaraj, I Kaleel, E Carrera, and M Petrolo. Nonlinear analysis of compact and thin-walled metallic structures including localized plasticity under contact conditions. *Engineering Structures*, page 109819, 2019.

[24] MH Nagaraj, J Reiner, R Vaziri, E Carrera, and M Petrolo. Progressive damage analysis of composite structures using higher-order layer-wise elements. *Composites Part B: Engineering*, page 107921, 2020.

[25] MH Nagaraj, E Carrera, and M Petrolo. Progressive damage analysis of composite laminates subjected to low-velocity impact using 2d layer-wise structural models. *International Journal of Non-Linear Mechanics*, page 103591, 2020.

[26] KV Williams, R Vaziri, and A Poursartip. A physically based continuum damage mechanics model for thin laminated composite structures. *International Journal of Solids and Structures*, 40(9):2267–2300, 2003.

[27] C Mcgregor, N Zobeiry, R Vaziri, and A Poursartip. A constitutive model for progressive compressive failure of composites. *Journal of composite materials*, 42(25):2687–2716, 2008.

[28] C McGregor, N Zobeiry, R Vaziri, A Poursartip, and X Xiao. Calibration and validation of a continuum damage mechanics model in aid of axial crush simulation of braided composite tubes. *Composites Part A: Applied Science and Manufacturing*, 95:208–219, 2017.

[29] A Forghani, N Zobeiry, A Poursartip, and R Vaziri. A structural modelling framework for prediction of damage development and failure of composite laminates. *Journal of Composite Materials*, 47(20-21):2553–2573, 2013.

[30] A Forghani, A Poursartip, and R Vaziri. An orthotropic non-local approach to modeling intra-laminar damage progression in laminated composites. *International Journal of Solids and Structures*, 180:160–175, 2019.

[31] M Shahbazi. *An efficient virtual testing framework to simulate the progression of damage in notched composite laminates*. PhD thesis, University of British Columbia, 2017.

[32] M Shahbazi, R Vaziri, and N Zobeiry. An efficient virtual testing framework to simulate the interacting effect of intra-laminar and inter-laminar damage progression in composite laminates. In *Proceedings of the American Society for Composites: Thirty-First Technical Conference*, 2016.

[33] M Petrolo and E Carrera. Methods and guidelines for the choice of shell theories. *Acta Mechanica*, 231:395–434, 2020.

[34] Z Hashin. Failure criteria for unidirectional fiber composites. *Journal of applied mechanics*, 47(2):329–334, 1980.

[35] ZP Bažant and Oh BH. Crack band theory for fracture of concrete. *Matériaux et construction*, 16(3):155–177, 1983.

[36] N Zobeiry. *Extracting the strain-softening response of composites using full-field displacement measurement*. PhD thesis, University of British Columbia, 2010.

[37] N Zobeiry, R Vaziri, and A Poursartip. Characterization of strain-softening behavior and failure mechanisms of composites under tension and compression. *Composites Part A: Applied Science and Manufacturing*, 68:29–41, 2015.

[38] J Reiner, N Zobeiry, and R Vaziri. A stacked sublaminate-based damage-plasticity model for simulating progressive damage in composite laminates under impact loading. *Thin-Walled Structures*, 156:107009, 2020.

[39] J Reiner and R Vaziri. Progressive axial crushing of composite laminates: A comparison between ls-dyna continuum damage models. In *Proceedings of the American Society for Composites—Thirty-third Technical Conference*, 2018.

[40] T Feser, J Reiner, R Vaziri, N Zobeiry, M Waimar, D Schueler, and N Toso-Pentecote. Simulation of axial crushing of flat coupon specimens using two intralaminar damage models implemented in ls-dyna and abaqus/explicit. In *13th World Congress in Computational Mechanics*, 2018.

[41] J Lee and C Soutis. Measuring the notched compressive strength of composite laminates: Specimen size effects. *Composites Science and Technology*, 68(12):2359–2366, 2008.

[42] X Xu, Aakash P, X Sun, and MR Wisnom. An experimental study of scaling effects in notched quasi-isotropic carbon/epoxy laminates under compressive loads. *Composites Part A: Applied Science and Manufacturing*, 137:106029, 2020.